On Electronic Properties of Assemblies of Quantum Nanodots†

F. Remacle‡

Département de Chimie, B6, Université de Liège, B 4000 Liège, Belgium

Received: September 29, 1999; In Final Form: February 11, 2000

The electronic response of a 2D hexagonal array of quantum dots is computed as a function of the distance between the dots. The electronic properties result from the interplay between three factors: (i) the "inherent disorder" due to the size, shape, and environmental fluctuations of the dots, (ii) the coupling of adjacent dots, and (iii) the role of the Coulombic repulsion. The computations are carried out using a Pariser−Parr−Pople type Hamiltonian, which is fully diagonalized in a many-electron basis as a function of the interdot separation. At high compression, the dots nearly touch one another and the electronic response is dominated by the coupling between the dots. An Anderson-like delocalized to localized transition arises as the lattice is expanded because the interdot coupling decreases. When the dots are further apart, the electronic response is dominated by the Coulombic repulsion of electrons (of opposite spin) on a given dot. The latter gives rise to a Mott-type insulator to metal transition as the extended array is compressed. In addition, we also discuss the case where large fluctuations in size are able to overcome the Coulombic effects. For such arrays, the Mott-type insulator to metal transition is smeared out by the disorder effects. Moreover, at large interdot separation, the ground state is found to be ionic while for moderately disordered arrays, the ground state is covalent. Comparison is made with the experimental results of the Heath group.

1. Introduction

Designer solids, where the electronic properties of the "atoms" can be tuned[1,2] and the related problem of molecular electronics[3,4] are receiving considerable attention. Key and current aspects can also be found in other papers in this special issue. I discuss a quantum mechanical computational approach where the following experimental and theoretical aspects are emphasized:

i. Role of Disorder. Assemblies of nanodots are particularly sensitive to the lack of perfect periodicity in the properties of the sites because the individual dots are inherently not identical. The reason is that the dots are prepared by wet chemical methods[5−8] and so there is some (possibly small, about 10% in diameter,[9] but always finite) fluctuation in the size of the dots. Since the electronic response of an individual dot is governed by its size,[10] the arrays always exhibit some inherent disorder and this is the case for both metallic dots and semiconducting ones.[11] The role of this disorder will be shown to be paramount, particularly so at closer packing.[12,13] In other words, there are qualitative changes in the electronic response of the supperlattice due to this disorder.

In addition to this inherent disorder, four additional contributions can be included in the present approach. The second source of disorder is a packing or "geometrical" disorder. This arises because the lattice need not be perfectly arranged or, even, it can be quite defectively packed. The computational results, to be discussed below, are that it takes a fairly extensive geometrical disorder before it induces qualitative changes in the electronic properties.

The third source of disorder is what one might call a chemical disorder, but one should recognize that the size distribution also has a chemical (or, to be strict, a thermodynamic) origin. By a chemical disorder[13] we mean that the chemical composition of the dots need not be uniform. To a large extent, whether this source of variation is present or not is under the control of the experimentalist.

The fourth source of perturbation is due to the thermal motion of the lattice. We mean here the changes in the inter-dot distances. The dots are heavy on the atomic scale and this means that the phonon frequencies are low so that the lattice vibrational modes are essentially classical with an average of kT thermal energy per mode. This effect is the same as that giving rise to resistivity in metals and to the polaron theory in crystals.[14,15] The formalism to be discussed below, while quantum mechanical, can incorporate this coupling and it can do so particularly easily in the limit when the motion of the lattice can be regarded as a classical field which is coupled to the electronic motion. As I will briefly discuss, in this limit the effect is not dissimilar to that due to geometrical disorder. I will not, however, present computational results for thermally assisted charge hopping from one dot to another.

The fifth perturbation discussed here is one that is more special to assemblies of nanodots. It is that the dots have an internal structure and the conducting electrons, as they move from one dot to another can scatter due to the internal degrees of freedom. The formalism can allow each dot to have its own set of electronic levels, but I will here adopt a modest approach and only allow phenomenologically for this effect by adding a scattering phase shift when an electron hops from one dot to another. More work is needed on the importance of this effect, which causes a dephasing of the coherent propagation of the electrons. Ultimately, the fourth and fifth effects can cause a transition from coherent to dissipative transport of charge.

ii. Role of Lattice Compression. Assemblies of nanodots provide a theorist's dream in that the coupling between the dots can be tuned over a wide range by experimentally varying the

† Part of the special issue "Electronic and Nonlinear Optical Materials: Theory and Modeling".

‡ Chercheur Qualifié, FNRS, Belgium. E-mail address: fremacle@ulg.ac.be. Fax: 32-4-3663413.

10.1021/jp993494z CCC: $19.00
Published on Web 04/15/2000

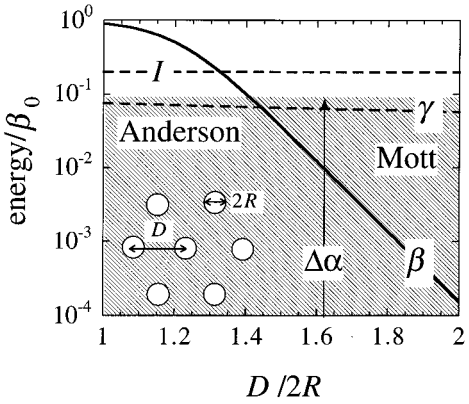

Figure 1. Relative strengths of the different perturbations included in the PPP Hamiltonian (2.12) as a function of the interdot separation $D/2R$, plotted on a logarithmic scale. $\Delta\alpha$ is the range of the fluctuation in the site energies and I the self-capacitance of the individual dots. The transfer integral, β, is given in eq 2.4 and the cross capacitance, γ, in eq 2.10. Note how the Coulombic effects and/or the fluctuation in the site energies are the strongest perturbation at large interdot separations, while it is β that plays a dominant role at small values of $D/2R$. The inset shows the two geometrical parameters of the 2D hexagonal array. D is the distance between the centers of two neighboring dots and $2R$ is the mean diameter of the dots.

lattice spacing. The details of doing so have been discussed elsewhere.[1,2,6] The range of variation is seemingly limited. The lattice spacing, D, that is, the distance between the centers of two adjacent dots (see inset in Figure 1) can be varied from about twice the mean diameter of the dots, $2R$, down to where the dots are effectively touching, $2 \geq D/2R \geq 1$. Even so, the experimental results in themselves[6,16,17] show that there are qualitative changes in the electronic and optical responses as the lattice spacing is varied in this range. Our analysis[12,13] of these results suggests that this is quite consistent with what one should expect considering the physical range of the inter-dot coupling.

There are two ways that the lattice spacing appears in the Hamiltonian. One, mentioned above, is that it governs the tunneling (or the above barrier transfer) of an electron from one dot to another. The second role of the inter-dot separation is that it governs the magnitude of the Coulombic repulsion between electrons localized on neighboring dots. This, which is a polarization or a cross-capacitance effect, is explicitly included in the Hamiltonian.

The experiments on the compressed lattice are static: The compression is changed very slowly. But the same Hamiltonian that allows us to compute the electronic response at different spacings can also be used to explore the dynamical role of the lattice motion.

iii. Coulomb Blockade. The computational scheme that we implement does fully and correctly incorporate the role of the, so-called, Coulomb blockade.[18−21] This, sometimes known as the "charging energy", is the energetic discrimination against two electrons (of opposite spin) being on the same dot. Often the effect is also referred to as the finite capacitance of a dot. The value of the charging energy can be determined experimentally by Coulomb blockade experiments.[2,22,23] Note that the capacitance is related to the volume of the dot and so it too can have a variation due to the fluctuations in size, to a lesser extent though than the fluctuations of the site energies (see below).

It is well-known how to write down a Hamiltonian that incorporates the Coulomb blockade. In solid state physics this is usually known as the Hubbard term.[24] Theoretical chemists are also aware of the importance of this effect and the equivalent Hamiltonian is known to them as that of Pariser−Parr−Pople (PPP).[25−30] The PPP Hamiltonian goes one step beyond the Hubbard model in that it also allows an electron on one dot to interact with an electron on another dot. These additional terms are expected to decrease in magnitude as the lattice spacing increases.

The electrostatic terms depend on two electrons at a time and so cannot be exactly treated in a one-electron approximation (also called the independent particle model or, technically, the self-consistent-field approximation). The computational scheme we use fully accounts for these terms. There is, of course, a price. We use a many-electron description of the wave function. Technically, we use a basis of states generated by the unitary group $U(n)$, where n is the number of dots in the array. The states are antisymmetrized spin eigenfunctions of a given multiplicity. The matrix elements of the electrostatic terms can be analytically computed in such a basis.[26,31] The price: the number of basis states (and hence the size of the Hamiltonian matrix) increases exponentially with n; cf. eq A.1 below. The advantage: when the Hamiltonian matrix is diagonalized, one (numerically) generates exact eigenstates. The band structure, including the relative positions of the valence and the conduction bands is thereby obtained.

Having enumerated the features that are included in the model Hamiltonian used herein, it is only reasonable to reiterate an important feature that is not properly handled. The Hamiltonian, as actually used in the present computations, does not do justice to the internal structure of the dots. To be sure, one can allow phenomenologically for this structure (we do say more about this below) and one can readily generalize the Hamiltonian as used here so as to endow each dot with an internal electronic structure. But this is yet to be implemented as a computationally viable scheme. (The problem is at the same time to do a proper job on the Coulomb blockade and to allow for an internal structure. The computational cost of doing so is that the size of the Hamiltonian matrix becomes prohibitive.)

2. Electronic Model

Each quantum dot is represented as a site of a lattice. In the computations reported below, there is one site orbital that can accommodate zero, one, or two (of opposite spin) electrons but, otherwise, the dot is not endowed with an internal structure. However, we will introduce some effects of the structure of the dot in eq 2.7 below, but this is done in a phenomenological manner.

The sites are arranged in a 2D hexagonal lattice, which means that completed shells have 7, 19, 37, 61, 91, ... sites, respectively. The geometry of the lattice is specified by D, the distance between the centers of adjacent dots where D is measured in units of $2R$. R is the mean dot radius, with a typical value of a few tens of ångstroms. The geometry of the 7 site lattice is shown as an inset in Figure 1.

Four unit-bearing coupling parameters determine the electronic properties of the lattice. These are shown in Figure 1, as a function of the lattice spacing measured in units of the mean diameter of the dots, $D/2R$. As indicated in the figure, the relative magnitude of these parameters determine the coupling regime. Two parameters characterize a given site. First are the site energies, α_i, $i = 1, 2, ..., n$. α is the energy of one electron in the site orbital. The site energies depend on the size of the dots and their inherent fluctuations, $\Delta\alpha$, and of course, on the chemical composition. α is expected to depend on the mean radius of the dots, R, as $1/R^2$, so that $\Delta\alpha \propto \alpha\, \Delta R/R$. Note that

the sites are coupled to one another so that the site energies are just a zeroth-order approximation for the energy of an electron on the site. When two electrons (of opposite spin) are localized in a given site orbital, the energy of the site is not 2α but $2\alpha + I$, where I, the self-capacitance, is the Coulombic repulsion of two electrons of opposite spin localized on the same site. I, which corresponds to the charging energy of the individual dots, can be determined by "Coulomb blockade" experiments, using scanning tunneling microscopy (STM).[2,22,23] I is size dependent. More precisely, $I = e^2/C(R)$, where e is the unit charge and $C(R)$ is the size dependent finite capacitance of an individual dot. $C(R) = 4\pi\epsilon_0\epsilon R$, where R is the radius of the dot, ϵ_0 is the permittivity of vacuum, and ϵ is the dielectric constant of the material surrounding the particle. ϵ is basically the dielectric constant of alkane chains of the ligands that stabilize the metallic core and varies between 2 and 3. For a 3 nm diameter quantum dot surrounded by a material with a dielectric constant, $\epsilon = 3$, I is found to be about 0.3 eV, which is in agreement with the Coulomb blockade experiments,[22] and we use this experimental value in the computation reported below. Because of the fluctuation in the mean dot radius, the charging energy also fluctuates. However, the range, $\Delta I \propto I\,\Delta R/R$, of the fluctuation in the charging energies remains small compared to the fluctuations of the site energies because I is typically more than an order of magnitude smaller than the site energies α. The effect of the fluctuation of the charging energies is therefore neglected in the computational results presented below.

Two parameters characterize the coupling of the dots and are therefore sensitive to the lattice spacing. The electron can coherently (but see below) transfer from one site to another with an amplitude β. The "transfer integral" β is determined by the overlap of the orbitals of adjacent dots and is therefore here put equal to zero unless the dots are near neighbors on the lattice. The value of β can be tuned by compressing the lattice and we expect it to decrease (exponentially) as the lattice is expanded (cf. Figure 1 and eq 2.4 below). For chemical physicists, an important role of the computation and of the comparison with experiment is to determine the decline of β with distance. We have previously done so[12] by fitting our computed response to the nonlinear optical response measured for an array of silver quantum dots.[6] β is also sensitive to the size of the dots and to the ligand coverage on the dots. Below, it will also be used to mimic the effect of lattice thermal motion and the internal structure of the dots (see eq 2.7).

The cross capacitance γ also couples adjacent dots. This electrostatic coupling is due to an electron on one dot polarizing a neighboring dot. It is usually not included in the Hubbard Hamiltonian but it is part of the PPP Hamiltonian. The cross capacitance is easy to incorporate because, like the self-capacitance, it is diagonal in the many-electron basis set that we use. The specific details are provided in the Appendix.

The form of the many-electron Hamiltonian is

$$H = H_0 + H_1 \tag{2.1}$$

H_0 is a one-electron Hamiltonian of the tight binding (or Hückel) type and allows for size fluctuations and lattice compression as discussed below

$$H_0 = \sum_{i,j}^{n} h_{i,j} \sum_{\mu}^{2} a_{i,\mu}^{\dagger} a_{j,\mu} \qquad \text{with}$$
$$h_{i,j} = \begin{cases} \alpha_i & \text{if} \quad i = j \\ \beta_{i,j} \neq 0 & \text{for near neighbors only} \end{cases} \tag{2.2}$$

where i is the index of a dot, $i = 1, 2, \ldots, n$. $a_{i,\mu}$ and $a_{i,\mu}^{\dagger}$ are the annihilation and creation operators for an electron on site i with a given spin μ (μ is up or down).[28,29] Note that while H_0 is a one-electron operator, H_1, which corresponds to the Coulombic terms (cf. eq 2.8 and section 2.2 below) is not.

2.1. One-Electron Considerations. Already at the level of H_0 one can see the effects of disorder, particularly so when the lattice is compressed, so that (see Figure 1) the role of the transfer integral β dominates. For the computations discussed below, we used α_i's that fluctuate randomly within $\Delta\alpha$ ($\equiv\alpha_0\delta\alpha$) around a mean value α_0:

$$\alpha_i = \alpha_0(1 + \delta\alpha_i) \equiv \alpha_0[1 + \delta\alpha(\mathrm{ran}_i - 0.5)] \tag{2.3}$$

where ran_i is a random number in the range of [0, 1] and the sampling is such that $\sum_i (\mathrm{ran}_i - 0.5) = 0$. The transfer integral β has the distance dependence

$$\beta = (\beta_0/2)(1 + \tanh((D_0 - D)/4RL)) \rightarrow \beta_0 \exp(-D/2RL) \tag{2.4}$$

which saturates at high compressions and otherwise has an exponential decline with a (dimensionless) range parameter L. The parameters of β in eq 2.4 are determined as discussed in ref 12 (see also Figure 1 therein), by a fit of the computed response to the experimental nonlinear optical response, the second harmonic generation (SHG).[6] For dots with a mean diameter $2R \approx 30$ Å, the fit of the experimental data[12] leads to $D_0/2R = 1.2$, which is the interdot separation by which β has dropped to half its maximal value, $\beta_0 = 0.5$ eV and $^1/_2L = 5.5$. The transfer integral is thus found to be rather long range. This value is consistent with what we estimate on the basis of a through space charge transfer.[13] Note that these parameters, determined by a fit to the experimental SHG,[12] lead also to a good agreement between the computed[32] and the experimental[17] response for another observable, the frequency dependent dielectric constant in the visible range. In particular, our model computations[32] reproduce the qualitative changes experimentally observed in the frequency dielectric constant, which exhibits the insulator to a metal transition as the lattice is compressed.[17]

When there are no fluctuations, the one-electron Hamiltonian of a lattice of identical dots can be written as[13]

$$h_{\text{Hückel}} = \alpha_0\mathbf{I} + \beta\mathbf{M} \tag{2.5}$$

where $\mathbf{M}$ is the $n \times n$ adjacency matrix (n is the number of sites),[33] i.e., a matrix with unit entries where the row and column indices correspond to near neighboring sites. The eigenvectors of $h_{\text{Hückel}}$ are the molecular orbitals (MO's). They are the eigenvectors of $\mathbf{M}$ and so do not change in character as the lattice spacing is changing. This is unlike when the fluctuation in the site energies are taken into account, where due to fluctuations, the MO's ($\equiv$eigenvectors of $n \times n$ H_0 (eq 2.2)) at low β ($=$large spacing) are localized.[13] This is the well-known Anderson transition[18−20,34] which occurs (cf. Figure 1) when the transfer integral β is no longer comparable in magnitude to the range of the fluctuations in the site energies. Then β cannot bridge the gap between the energies of adjacent sites and the one-electron wave function becomes localized. This remains also the case in the equivalent many-electron Hückel description, as can be seen from Figure 2, which shows the weights of the ground state on the zeroth-order many-electron site states for two interdot separations. At each interdot separation, the weights result from a full diagonalization of the Hückel Hamiltonian in the many-electron basis set (for the details about the many-

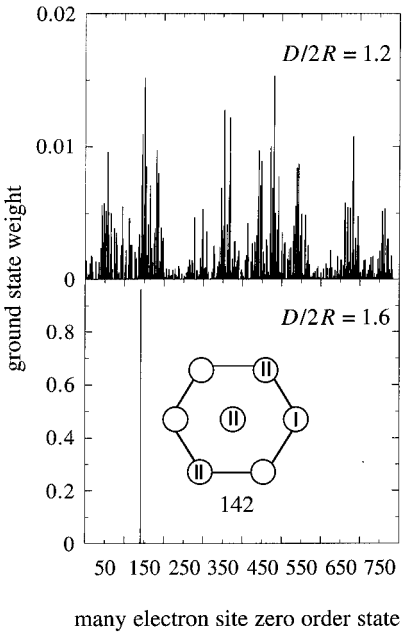

Figure 2. Weights of the many-electron ground electronic state of the Hückel Hamiltonian (eq 2.2) on the 784 many-electron site states, computed for $D/2R = 1.2$ (upper panel) and $D/2R = 1.6$ (lower panel). $\alpha_0 = 20\,\beta_0$, $\Delta\alpha = 1\,\beta_0$, and the parameters in β are as given in section 2.1. At short interdot separation, the ground electronic state is well delocalized over the site many-electron states. At larger interdot separation, the ground electronic state becomes localized on a single site many-electron state.[35] Note the difference of scale for the *y* axis in the upper and the lower panels.

electron description, see section 2.2). At short interdot separation (upper panel), β is the strongest perturbation. The ground electronic state is well delocalized over all the many-electron site states of a given total spin, and the array has a metallic character. On the other hand, at large interdot separation, β is orders of magnitude weaker than the fluctuation in the site energies. Then, the ground electronic state converges to a single ionic state (state number 142,[35] the state numbering is arbitrary), whose site occupancies are uneven, as shown in the inset. The convergence of the Hückel ground electronic state to an ionic configuration at large separation in the presence of site energy fluctuation is due to the failure of the Hückel Hamiltonian to discriminate between the covalent and the ionic many-electron states. This is further discussed in sections 2.2 and 3 below where eqs 3.1−3.4 provide a schematic representation of the site occupancy of the covalent and ionic many-electron states.

Geometrical disorder implies fluctuation in the magnitude of β. Both the analytical and computational evidence[13] is that this is not such an important effect. The reason is the exponential dependence of β on the lattice spacing. From eq 2.4

$$\frac{|\delta\beta|}{\beta} \xrightarrow{D>R} \delta\left(\frac{D}{2R}\right)\Big/L = \left(\delta\left(\frac{D}{2R}\right)\Big/\left(\frac{D}{2R}\right)\right)\left(\left(\frac{D}{2R}\right)\Big/L\right) \quad (2.6)$$

Large variations in the lattice spacings will cause large changes in β at large interdot separations, where the value of β becomes negligible with respect to the charging energy, I, and the range of the fluctuation in the site energies, $\Delta\alpha$.

Before turning to a many-electron theory, we point out two additional sources of variations in β. One is the role of lattice thermal vibrations. So far we discussed the lattice spacing as a parameter in the Hamiltonian. Strictly speaking, however, it is a dynamical variable and, in a quantum mechanical approach, it is an operator. It is, of course, simpler to regard the lattice vibrations as classical. Then, D becomes a time dependent variable, of bounded variation, whose mean value is the nominal lattice spacing and whose variance is determined by the equipartition theorem. It is therefore easy to compute $\langle\beta\rangle$ where the mean is a thermal average. However, what we really need to do is to compute $\langle\exp(-iHt)\rangle$. This is possible and we will report on it elsewhere.

The internal structure of the dots is also a source of modulation of β. In the one-electron picture, the migrating electron moves into or out of the site orbital. In reality, the electron is scattered within the dot (as seen, e.g., in the width of the plasmon resonance[6,36]). Even if the scattering is elastic, the electron acquires an extra phase and this phase can be quite different for different dots. It follows that the simplest correction for the role of the internal structure is to replace the otherwise real β by a complex number, whose phase is essentially random and which, in lowest order, allows only for elastic event so that the matrix $\boldsymbol{\beta}$ should remain Hermitian

$$\beta_{ij} \rightarrow |\beta| \exp(i\delta_{ij}) \qquad \beta_{ji} = \beta_{ij}^{*} \quad (2.7)$$

This does not require any additional computational effort because the Hamiltonian remains Hermitian and so can be diagonalized by a unitary transformation. Such computations have just been reported.[37]

2.2. Many-Electron Theory. This section discusses the exact incorporation of two-electron effects, such as Coulomb blockade, by using a many-electron wave function. The form of the many-electron Hamiltonian is

$$H = H_0 + H_1 \quad (2.1)$$

where H_0 is the one-electron Hamiltonian of the Hückel (or tight binding) part as given by eq 2.2. Then

$$H = \underbrace{\sum_{i,j}^{n} h_{ij} \sum_{\mu}^{2} a_{i,\mu}^{\dagger} a_{j,\mu}}_{\text{one-electron part}} + \underbrace{\frac{1}{2} I \sum_{i} (n_i - 1)^2}_{\text{Coulomb blockade}} + \underbrace{\frac{1}{2} \gamma \sum_{i,j} n_i n_j}_{\text{cross polarization}} \quad (2.8)$$

where the new operators that enter are the number operators for the different sites, $i = 1, 2, \ldots, n$,

$$n_i \equiv \sum_{\mu} a_{i,\mu}^{\dagger} a_{i,\mu} \quad (2.9)$$

which sums over both directions of the spin. The parameters of the one-electron part are as discussed in section 2.1, determined by a fit to the experimental nonlinear optical response.[12] I is the charging of the individual dots, also discussed above. We use for the variation of the cross capacitance, γ, with the interdot separation the same weak distance dependence as in molecules,[38]

$$\gamma = e^2/[2R(D/2R + (e^2/I2R) + a)] \quad (2.10)$$

where a is a constant and e is the unit charge. Note that the magnitude of the cross polarization term is typically weaker than the Coulomb blockade term and does not play an important role in the computational results reported below.

To diagonalize this Hamiltonian exactly (which is equivalent to a full configuration interaction (CI)), we rewrite it in terms of the generators, $\hat{E}_{i,j}$,

$$\hat{E}_{i,j} \equiv \sum_{\mu}^{2} a_{i,\mu}^{\dagger} a_{j,\mu} \qquad i, j = 1, ..., n \tag{2.11}$$

of the unitary group $U(n)$ (n is the number of sites).[26,27,31,39,40]

$$H = \alpha_0 \sum_{i=1}^{n} (1 + \delta\alpha_i)\hat{E}_{i,i} + \beta \sum_{i,j}^{n}{}' \hat{E}_{i,j} + \frac{I}{2} \sum_{i=1}^{n} (\hat{E}_{i,i} - 1)^2 + \frac{\gamma}{2} \sum_{i,j}^{n} \hat{E}_{i,i}\hat{E}_{j,j} \tag{2.12}$$

The prime on the second sum indicates that i and j are near neighbors. Note that only diagonal operators appear in the two-electron terms. As discussed in the Appendix, this makes the analytical form of the Hamiltonian matrix quite simple. In particular, the site-diagonal part,

$$H_{\text{site}} = \alpha_0 \sum_{i=1}^{n} (1 + \delta\alpha_i)\hat{E}_{i,i} + \frac{I}{2} \sum_{i=1}^{n} (\hat{E}_{i,i} - 1)^2 \tag{2.13}$$

is a diagonal matrix. For the n-electron n-site system that we consider here, the Coulomb blockade term ($(^1/_2)\Sigma(\hat{E}_{ii} - 1)^2$) counts the number of doubly occupied sites. The reason is that in this particular case, the number of doubly occupied orbitals is equal to the number of unoccupied sites.

Specifically, we represent the Hamiltonian in a spin adapted many-electron basis set that belong to an irreducible representation of the group $U(n)$[39](Gelfand − Teltsin states). There are 784 such (doublet) states for a 7-electron, 7-site lattice. For the next completed hexagon there are 19 sites and 2 821 056 160 doublet states. (The required equation is (A.1) of the Appendix where more detail is provided about the many-electron states).

3. Results for a Many-Electron Description

Before reporting results for the full diagonalization of the Hamiltonian (2.8), we first discuss the properties of the electronic spectrum at large values of the interdot separation, $D/2R$, where the strength of the transfer integral, β, is much smaller than the Coulomb terms (cf. Figure 1) so that it can be neglected. Then, at large interdot separation, the electronic spectrum exhibits a band structure that can be understood in terms of the Hamiltonian H_{site} (eq 2.13). Note that the cross polarization term of eq 2.8 is neglected in (2.13). This provides a simpler discussion and does not affect the band structure. The reason is that, typically, the cross capacitance, γ, is smaller than the self-capacitance, I. As a result, the effect of the cross polarization term is essentially to shift the levels within the bands that are separated by the charging energy, I.

H_{site} is diagonal in the many-electron site basis set. Without the Coulomb repulsion term and in the absence of fluctuations in the site energies ($\delta\alpha = 0$), all the doublet states of an n-site, n-electron model are degenerate with an energy $n\alpha_0$. For $n = 7$, the possible electronic configurations have zero, one, two, or three doubly occupied sites. Since each doubly occupied orbital is penalized by I because of the Coulombic repulsion, when the Coulomb blockade term is included, four bands of degenerate states appear with energies $7\alpha_0$, $7\alpha_0 + I$, $7\alpha_0 + 2I$, and $7\alpha_0 + 3I$, respectively. The zeroth-order ground state corresponds to the electronic configurations with one electron per site (see eq 3.1 below) and is unaffected by the Coulomb blockade term. It is 14 times degenerate, and its energy is $7\alpha_0$. It is a covalent state that has an insulator character because the matrix elements of the transfer integral β among these 14 degenerate states are zero. All the excited electronic states are ionic (they have at least a doubly occupied site orbital). They will be coupled by β when it is strong enough to bridge the gaps between their respective energies. (For the ionic zeroth-order states, the matrix $\boldsymbol{\beta}$ has both interband and intraband nonzero matrix elements.) Equations 3.1−3.4 show the occupancies of the seven site orbitals for one of the degenerate many-electron states belonging to each of the four bands.

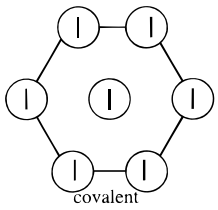

$$E_g = 7\alpha_0 \tag{3.1}$$

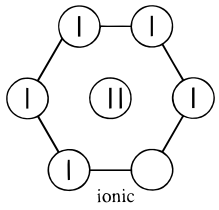

$$E_1 = 7\alpha_0 + I \tag{3.2}$$

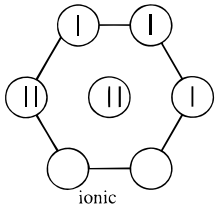

$$E_g = 7\alpha_0 + 2I \tag{3.3}$$

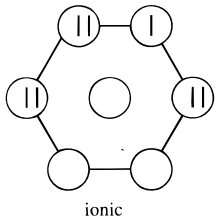

$$E_g = 7\alpha_0 + 3I \tag{3.4}$$

As already discussed, the covalent ground state (eq 3.1) is 14 times degenerate. There are 210 degenerate ionic states with an energy equal to $7\alpha_0 + I$ (eq 3.2), which are all the doublet configurations with a single doubly occupied site orbital, 420 ionic states at $7\alpha_0 + 2I$ (two doubly occupied site orbitals, eq 3.3), and 140 ionic states at $7\alpha_0 + 3I$ with three doubly occupied site orbitals (eq 3.4).

Fluctuations in the site energies are diagonal in the zeroth-order many-electron site states. They do not affect the ground electronic state since the sampling is such that $\sum_i(\text{ran}_i - 0.5)$. Therefore, its energy remains unchanged and equal to $7\alpha_0$ even when disorder is taken into account. On the other hand, the energy mismatch in the site energies due to disorder splits the energies of the ionic states, which leads to a smear out of the band structure of the higher states, as can be seen in Figure 3 below.

The upper panel of Figure 3 shows the transition frequencies, $E_{\text{ng}} = E_{\text{n}} - E_{\text{g}}$, where E_{g} is the energy of the ground electronic state and E_{n} is the energy of the electronic excited state, computed for moderate fluctuation in the site energies, that is, for a range of fluctuation, $\Delta\alpha$, that is smaller than the self-capacitance of the individual dots, I: $\Delta\alpha < I$. The transition frequencies are computed by full diagonalization of the PPP Hamiltonian (2.12) as a function of the interdot separation $D/2R$. The details of the full CI procedure that we implement are given in the Appendix. At large values of $D/2R$, as discussed above, H_{site} (eq 2.13) is a good description. One clearly sees the band of 13 very small transition frequencies arising from the splitting of the 14 times degenerate zeroth-order covalent ground state by the second-order (and higher) terms of the transfer integral, which leads to transition frequencies of the order of β^2/I. The

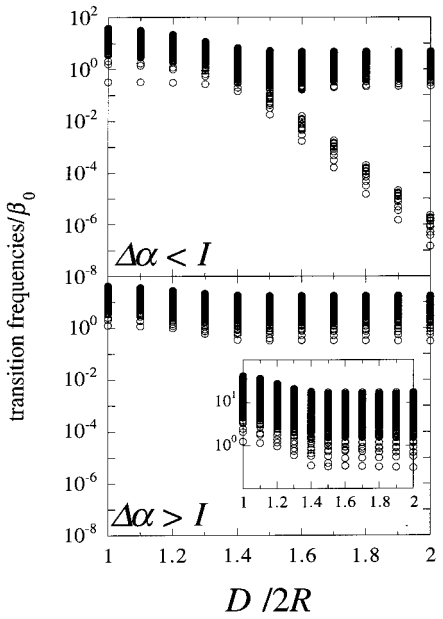

Figure 3. Transition frequencies, $E_{ng} = E_n - E_g$, in units of β_0, computed as a function of the interdot separation $D/2R$. The parameters used are $\alpha_0 = 20\ \beta_0$ and $I = 1.2\ \beta_0$ and γ is given in eq 2.10 with $2R = 30$ Å and $a = 1$ Upper panel: $\Delta\alpha < I$ ($\Delta\alpha = 1\ \beta_0$). The Mott transition occurs at $D/2R \approx 1.5$, and the Anderson-like transition, at $D/2R \approx 1.3$. Lower panel: $\Delta\alpha > I$ ($\Delta\alpha = 5\ \beta_0$). In this case, the Mott transition is smeared out by the fluctuation in the site energies. In the inset, the E_{ng}'s are shown for a smaller energy range. The Anderson transition is seen to occur at a smaller value of $D/2R$ ($D/2R = 1.2$) than in the upper panel.

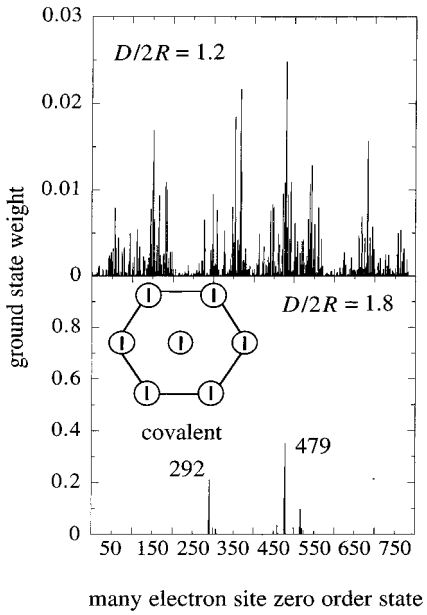

Figure 4. Weights of the ground electronic state on the many-electron site zeroth-order states for an array where $\Delta\alpha < I$. Computed for the same Hamiltonian parameters as in Figure 3 upper panel. Upper panel: $D/2R = 1.2$. The wave function is well delocalized over all the 784 many-electron site zeroth-order states. Lower panel: $D/2R = 1.8$, the ground electronic state converges to a linear combination of the 14 covalent site zeroth-order states, with the highest weights on states 219 and 479. The inset shows the site occupancy of the covalent states. Note the difference of scale for the *y* axis in the upper and the lower panels.

three higher bands have merged into a single band of ionic states because of the fluctuations in site energies and also because of the cross polarization term. They are separated from the ground state by an energy gap at least equal to I. As the interdot separation decreases, the strength of the transfer integral, β, increases exponentially (eq 2.4 and Figure 1) and when it is strong enough to overcome the Coulombic effects, the lower covalent band merges with the higher ionic bands. This is the Mott transition and it occurs for the parameters of our model at $D/2R = 1.5$.

Therefore, for $D/2R > 1.5$, the array behaves as a Mott insulator, with a covalent ground state. This can be seen from the lower panel of Figure 4 where the weights of the ground electronic state on the zeroth-order many-electron site states are plotted for $D/2R = 1.8$. The ground electronic state is found to be a linear combination of the 14 covalent zeroth-order site states (eq 4.1), with larger weights on states 292 and 479 (the numbering of the states is arbitrary).[35] This is unlike for the many-electron Hückel Hamiltonian, where the ground many-electron state shown in Figure 2 converges to an ionic configuration at large interdot separation. Figure 2 and Figure 4 are computed for the same amount of disorder in the site energies. The difference is that in the Hamiltonian used in Figure 4, the Coulombic terms (Coulomb blockade and cross polarization; see eq 2.8) are included. As a result, and insofar that $\Delta\alpha < I$, the ground electronic state is covalent, because the Coulomb blockade term penalized the ionic configurations by I (the "charging energy") for each doubly occupied orbital. On the other hand, in the Hückel Hamiltonian, there is no energy penalty for doubly occupied sites, so that covalent and ionic configurations are degenerate (of course here within the range of the fluctuation in the site energies). This is a well-known failure of the one-electron description.[41]

The upper panel of Figure 4 shows the weights of the ground state computed for a smaller value of the interdot separation ($D/2R = 1.2$). For this interdot separation, the electronic coupling, β, is strong enough to bridge the Coulombic effects and the fluctuations in the site energies, so that the ground state is very well delocalized over all the site zeroth-order states. For these small values of $D/2R$, the array is conducting. The Anderson-like transition is found to occur at a value of $D/2R \approx 1.3$. The smallest transition frequency ($E_{ng} \approx 0.4\ \beta_0$) seen in Figure 3 upper panel at short distances ($D/2R < 1.3$) is due to the splitting of the doubly degenerate zeroth-order ground state (≡ground state of the Hamiltonian (2.5)) by the fluctuation in the α_i's.

In the lower panel of Figure 3, the transition frequencies are plotted for a larger amount of fluctuation in the α_i's, so that $\Delta\alpha > I$, for the same range in the energy axis as in the upper panel. At large interdot separation, the band gap between the covalent and the ionic many-electron states that is due to the Coulombic effects has vanished. This indicates that the Mott transition is smeared out by the fluctuation in the site energies: For larger amounts of disorder, the very small transition frequencies (of the order of β^2/I) disappear and the distribution of transition frequencies is entirely determined by the range of fluctuation in the site energies, $\Delta\alpha$. The inset in the lower panel is for a smaller range in energy, so that the details of the distribution of the transition frequencies appears more clearly. Note that since $\Delta\alpha$ is wider, the Anderson transition occurs at a shorter value of $D/2R$ ($D/2R = 1.2$) because a larger value of β is needed to bridge the energy mismatch between the site energies.

At large interdot separations, as $\Delta\alpha$ increases, an interesting transition occurs for the ground electronic state: While for $\Delta\alpha < I$ the ground electronic state is covalent (Figure 4, lower panel), larger amounts of disorder ($\Delta\alpha > I$) lead to an ionic

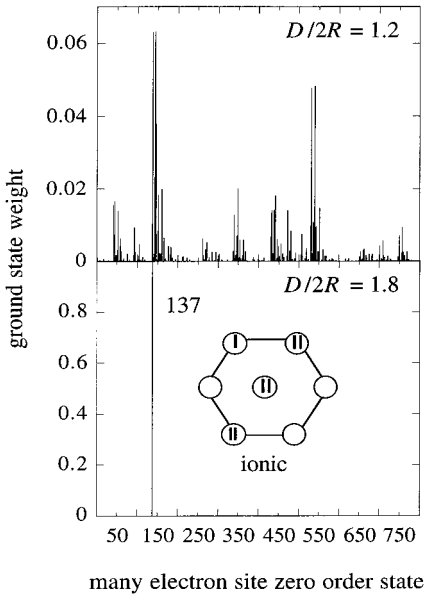

Figure 5. Weights of the ground electronic state on the many-electron site zeroth-order states for a highly disordered array with $\Delta\alpha > I$. Computed for the same Hamiltonian parameters as in Figure 3 lower panel. Upper panel: $D/2R = 1.2$. The wave function is still well delocalized over all the 784 many-electron site zeroth-order states. Lower panel: $D/2R = 1.8$. The ground electronic state now converges to an ionic state, the state number 137, whose site occupancy is shown in the inset.[35] Note the difference of scale for the *y* axis in the upper and the lower panel.

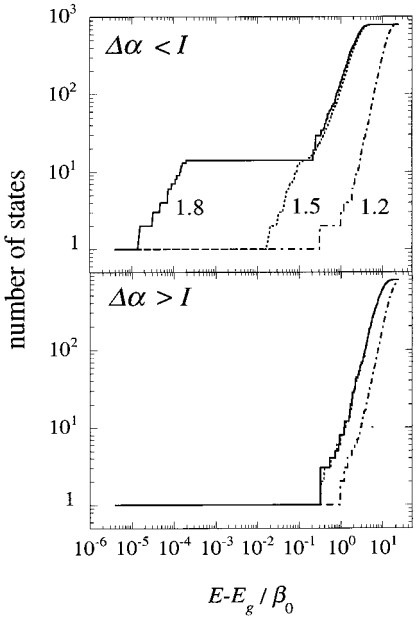

Figure 6. Number of states vs energy computed for three interdot separations: $D/2R = 1.8$, 1.5, and 1.2. Upper panel: $\Delta\alpha < I$ (same Hamiltonian parameters as in the upper panel of Figure 3). At large interdot separation, there is a gap in energy of about *I* between the 14 lowest covalent electronic states and the higher ionic states. Lower panel: $\Delta\alpha > I$ (same Hamiltonian parameters as in the lower panel of Figure 3) The gap has disappeared because the fluctuation in the site energies is wide enough to wash out the band structure due to the Coulombic effects.

ground electronic state (lower panel of Figure 5). The computation reported in Figure 5 is for the same Hamiltonian parameters as in the lower panel of Figure 3. The ground state computed at $D/2R = 1.8$ converges to the ionic state number 137, whose site occupancy is shown as an inset in the figure.[35] For smaller values of $D/2R$ (upper panel), the ground electronic state remains well delocalized over the whole range of many-electron zeroth-order site states. It is less well delocalized, though, than for the same value of $D/2R$ as in the upper panel of Figure 4 because $\Delta\alpha$ is larger in Figure 5.

In Figure 6, the number of states is plotted as a function of energy for three interdot separations, $D/2R = 1.2$, 1.5, and 1.8. For moderate amounts of disorder such that $\Delta\alpha < I$ (upper panel of Figure 6), at large interdot separation ($D/2R = 1.8$), the Coulomb gap between the 14 covalent states and the ionic bands is clearly seen. This gap can be probed experimentally by current−voltage ($I-V$) measurements on the arrays as a function of the interdot separation, from which density of state curves can be obtained.[2,22,23]At this large interdot separation, a more disordered array (such that $\Delta\alpha > I$) does not exhibit a gap in the number of states vs energy curve, as can be seen from the lower panel. The Mott insulator−metal transition is masked by the fluctuations in the site energies, which are strong enough to wash out the band structure induced by the Coulombic effects.

At large interdot separation, highly disordered arrays ($\Delta\alpha > I$) are expected to exhibit a finite density of states at 0 K since there is no Coulomb gap, but they still behave as an insulator because the transfer integral, β is not strong enough to bridge the energy mismatch between the different states due to disorder. Recent experimental results of the Heath group[17] on disordered bilayers, where the metallic character is probed by measuring the frequency dependent dielectric constant in the visible show that this can be the case. Another interesting feature of these disordered supperlattices is that individual dots in the array are expected to lead to different $I-V$ curves, as suggested by our model where ionic states have three different kinds of sites, with zero, one, and two electrons, respectively. This appears to be supported by recent experimental measurements[23,42] and work is in progress along these lines.[43]

4. Concluding Remarks

The compression of silver quantum dot arrays that is possible using the Langmuir technique allows reversible tuning of the strength of the interdot coupling. It therefore provides an experimental access to different facets of the insulator to metal transition, which occurs as the lattice is compressed.[1,2,6,16] Basically, the arrays behave as a metal at small interdot separations and have an insulator character at larger separations. One important aspect of the metal−insulator transition is that it can be reversed by decreasing the level of compression of the lattice. The metal to insulator transition in 2D monolayers of silver quantum dots has been probed by the Heath group using various experimental techniques: by optical means by measuring the second harmonic generation[6] and the frequency dependent dielectric constant in the visible[2,17] and at very low frequencies by impedance spectroscopy.[16] Variable temperature STM gives access to the Mott transition.[22,23]

The metal to insulator transition manifests itself by qualitative changes in the various experimental responses; i.e., the second harmonic generation measured in the visible increases exponentially as the lattice is compressed,[6] the real part of the complex frequency dependent dielectric constant becomes negative upon lattice compression,[17] and the Coulomb gap in the density of states observed for low temperature at large interdot separation disappears as the dots are brought closer.[22,23] The electronic model discussed here reproduces well these qualitative changes, and semiquantitative comparisons with the experimental results of the Heath group are provided elsewhere.[12,32] Here, we discussed more systematically the role of

the inherent disorder and of the Coulombic effects on the electronic properties using computational examples. A systematic discussion is possible because a small number of electronic parameters, that is, the variation of the transfer integral, β, with the interdot separation, the value of the charging energy, I, of the individual dots, and the range of the fluctuations in the sizes, ΔR, suffice to capture the essential features of the changes in electronic response as the lattice is compressed. Moreover, these parameters can be determined from experiment. As discussed in section 2, we take the experimental values of I and ΔR. The parametrization of β is determined from the fit of the computed response to the experimental second harmonic generation,[12] as also discussed in section 2. We would like to reiterate that the same values of these parameters, together with the experimental values of I and ΔR, also reproduce at a semiquantitative level the changes due to the metal to insulator transition experimentally observed for other quantities, such as the frequency dependent dielectric response[17,32] and the Coulomb blockade curves obtained by STM.[22,23,43]

Disorder is inherently present in supperlattices of quantum nanodots because of the inherent size fluctuation due to their preparation by wet chemical synthesis. Disorder plays an important role both in the Anderson type and in the Mott type metal to insulator transitions. It is the driving force for the Anderson-like transition that occurs when the interdot coupling is no longer strong enough to bridge the differences in the site energies induced by the size fluctuations. The Mott metal to insulator transition is also strongly affected by disorder. Our computational results show that it can be masked when the disorder in the site energies overcome the Coulombic terms. Depending on the amount of disorder, the Anderson type and the Mott type transitions do not occur at the same interdot separation. While optical measurements (SHG and frequency dependent dielectric constant) appear to be more sensitive to the Anderson transition, density of states (DOS) curves obtained by STM probe the presence (or not) of the Coulomb gap typical of the Mott insulators.

For arrays with moderate amounts of disorder ($\Delta\alpha < I$), we find that the Anderson-like transition occurs at a shorter interdot separation than the Mott transition. Intermediate values of $D/2R$ correspond to an intermediate coupling regime where all perturbations are important. Our computational results also show, in agreement with recent experiments,[17,22,23] that at large interdot separation, increasing amounts of disorder can induce a transition from a covalent to an ionic ground electronic state, thereby leading to arrays with no Coulomb gap at 0 K but still behaving as a insulator because of the Anderson localization of the wave function due to disorder. The $I - V$ curves of the individual dots belonging to such arrays with an ionic ground electronic state are expected to be of three kinds, corresponding to the three kinds of dots typical of an ionic ground state: neutral, with an excess of electron and with a defect of electron, as suggested by our many-electron model. Preliminary experimental results show that it is likely to be the case.[23,42]

Acknowledgment. I thank Professor R. D. Levine for his support and for many discussions, and Professor J. R. Heath, Dr. R. S. Williams, Dr. C. P. Collier, and Dr. S.-H. Kim for useful insights about their experimental results. The Commissariat général aux relations internationales de la Communauté française de Belgique (CGRI) and the Israeli Government are acknowledged for supporting my stay at the Fritz Haber Research Center in Jerusalem during the summer '99. This work used the computational facilities of SFB 377.

Appendix: The Site Many-Electron Basis Set and the Hamiltonian Matrix

The many-electron description that we implement is based on the "spin free" formalism pioneered by Paldus[26] and Matsen.[40] This formalism is based on a unitary group approach[39] that consists of rewriting the Hamiltonian in terms of the generators $\hat{E}_{i,j}$ (eq 2.11) of the group $U(n)$, where n is the number of sites. This leads to eq 2.12

The matrix of the Hamiltonian (2.12) is then written in the spin symmetry adapted many-electron site states. For a system of n sites and N electrons, of total multiplicity $(2S + 1)$, the dimension $\mathcal{N}$ of the irreducible representation of the spin symmetry adapted N-electron states is uniquely specified and given by

$$\mathcal{N} = \frac{b+1}{n+1}\binom{n+1}{a}\binom{n+1}{c} \tag{A.1}$$

where

$$\begin{aligned} a + b + c &= n \\ 2a + b &= N \\ b &= 2S \end{aligned} \tag{A.2}$$

and $\binom{m}{n}$ are the binomial coefficients. For the (n=) seven-site, (N=) seven-electron system there are $\mathcal{N} = 784$ many-electron doublet ($S = {}^1/_2$) states. (a, b, c) are the components of the highest weight vector in Paldus' notation. All the orthonormal spin-adapted N-electron states can be generated in terms of the (a, b, c) vector. For the $n = 7$, $N = 7$ system, this vector is (3, 1, 3) for all the 784 doublet states. One convenient way to represent the many-electron states is to write them as an n-row three-column Paldus tableaux where the highest row of the tableau is given by the highest weight vector $(a, b, c) \equiv (a_n, b_n, c_n)$. The entries of the different rows are then recursively obtained from the highest weight vector.[26,31]

The matrix elements of the Hamiltonian (2.12) in the site many-electron states, (m), take a very simple form. The diagonal generators $\hat{E}_{i,i}$ are diagonal:

$$\langle (m)|\hat{E}_{i,i}|(l)\rangle = e_i^{(m)}\,\delta_{(m),(l)} \tag{A.3}$$

where $e_i^{(m)}$ is the occupancy of site i for the many-electron site state, (m), $e_i^{(m)} = 0$, 1, or 2. This implies that all the Coulombic (two-electron) terms included in the Pariser−Parr−Pople Hamiltonian are diagonal in the site many-electron states. The only nondiagonal terms are the matrix elements of the transfer integral, β. They are readily computed using the matrix representation[26,31] of the near neighbor raising and lowering generators $\hat{E}_{i,i\pm1}$, $i = 1, ..., n - 1$, and the commutation relation

$$[E_{i,j}, E_{k,l}] = \delta_{j,k}E_{i,l} - \delta_{i,l}E_{k,j} \qquad i, j, k, l = 1, ..., n \tag{A.4}$$

which implies the recursion relation

$$\hat{E}_{i,j+1} = [\hat{E}_{i,j}, \hat{E}_{j,j+1}] \tag{A.5}$$

(A.5) is used to compute the matrix elements, $\hat{E}_{i,j\neq i\pm1}$, which are necessary for a 2D hexagonal structure.

The $\mathcal{N} \times \mathcal{N}$ ($\mathcal{N} = 784$) matrix of the Hamiltonian (2.12) is then diagonalized, which corresponds to a full CI diagonalization for PPP Hamiltonian.

References and Notes

(1) Collier, C. P.; Vossmeyer, T.; Heath, J. R. *Annu. Rev. Phys. Chem.* **1998**, *49*, 371.

(2) Markovich, G.; Collier, C. P.; Henrichs, S. E.; Remacle, F.; Levine, R. D.; Heath, J. R. *Acc. Chem. Res.* **1999**, *32*, 415.
(3) *Molecular Electronics*; Jortner, J., Ratner, M., Eds.; Blackwell Science: Oxford, U.K., 1997.
(4) Collier, C. P.; Wong, E. W.; Belohradsky, M.; Raymo, F. M.; Stoddart, J. F.; Kuekes, P.; Williams, R. S.; Heath, J. R. *Science* **1999**, *285*, 391.
(5) Brust, M.; Walker, M.; Bethell, D.; Schiffrin, D. J.; Whyman, R. *J. Chem. Soc., Chem. Commun.* **1994**, *1994*, 801.
(6) Collier, C. P.; Saykally, R. J.; Shiang, J. J.; Henrichs, S. E.; Heath, J. R. *Science* **1997**, *277*, 1978.
(7) Chen, S.; Ingram, R. S.; Hostetler, M. J.; Pietron, J. J.; Murray, R. W.; Schaaff, T. G.; Khoury, J. T.; Alvarez, M. M.; Whetten, R. L. *Science* **1998**, *280*, 2098.
(8) Murray, C. B.; Kagan, C. R.; Bawendi, M. G. *Science* **1995**, *270*, 1335.
(9) Heath, J. R.; Knobler, C. M.; Leff, D. V. *J. Phys. Chem. B* **1997**, *101*, 189.
(10) Bawendi, M. G.; Steigerwald, M. L.; Brus, L. E. *Annu. Rev. Phys. Chem.* **1990**, *41*, 477.
(11) Alivisatos, A. P. *Science* **1996**, *271*, 933.
(12) Remacle, F.; Collier, C. P.; Heath, J. R.; Levine, R. D. *Chem. Phys. Lett.* **1998**, *291*, 453.
(13) Remacle, F.; Collier, C. P.; Markovitch, G.; Heath, J. R.; Banin, U.; Levine, R. D. *J. Phys. Chem. B* **1998**, *102*, 7727.
(14) Mott, N. F.; Davis, E. A. *Electronic Processes in Noncrystalline Materials*; Clarendon Press: Oxford, U.K., 1971.
(15) Madelung, O. *Introduction to Solid-State Theory*; Springer: Berlin, 1996.
(16) Markovich, G.; Collier, C. P.; Heath, J. *Phys. Rev. Lett.* **1998**, *80*, 3807.
(17) Henrichs, S.; Collier, C. P.; Saykally, R. J.; Shen, Y. R.; Heath, J. R. *J. Am. Chem. Soc.*, in press.
(18) Mott, N. F. *Metal*−*Insulator Transitions*; Taylor & Francis: London, 1990.
(19) Imada, M.; Fujimori, A.; Tokura, Y. *Rev. Mod. Phys.* **1998**, *70*, 1039.
(20) Zallen, R. *The Physics of Amorphous Solids*; Wiley: New York, 1983.
(21) Kouwenhoven, L. P.; McEuen, P. L. In *Nanotechnology*; Timp, G., Ed.; Springer-Verlag: New York, 1999.
(22) Medeiros-Ribeiro, C.; Ohlberg, D. A. A.; Williams, R. S.; Heath, J. R. *Phys. Rev. B* **1999**, *59*, 1633.
(23) Kim, S.-H.; Meideiros-Ribeiro, G.; Ohlberg, D. A. A.; Williams, R. S.; Heath, J. R. *J. Phys. Chem. B* **1999**, *103*, 10341.
(24) Hubbard, J. *Proc. R. Soc.* **1963**, *276*, 238.
(25) Parr, R. G. *Quantum Theory of Molecular Electronic Structure*; Benjamin: New York, 1963.
(26) Paldus, J. *J. Chem. Phys.* **1974**, *61*, 5321.
(27) Matsen, F. A. *Int. J. Quantum Chem.* **1990**, *37*, 389.
(28) Schatz, G. C.; Ratner, M. A. *Quantum Mechanics in Chemistry*; Prentice Hall: New York, 1993.
(29) Linderberg, J.; Ohrn, Y. *Propagators in Quantum Chemistry*; Academic Press: New York, 1973.
(30) Koutecky, J. *Chem. Phys. Lett.* **1967**, *1*, 249.
(31) Paldus, J. In *The Unitary Group for the Evaluation of Electronic Energy Matrix Elements;* Hinze, J., Ed.; Lecture Notes in Chemistry, 22; Springer: Berlin, 1981.
(32) Remacle, F.; Levine, R. D. *J. Am. Chem. Soc.* **2000**, in press.
(33) *Free Electron Theory of Conjugated Molecules*; Platt, J. R., Ed.; Wiley: New York, 1964.
(34) Anderson, P. W. *Concepts in Solids*; Benjamin: Palo Alto, CA, 1971.
(35) For other draws of the fluctuations, the ground state converges to a different ionic state or to a superposition of ionic states in the case of accidental degeneracies.
(36) Farbman, I.; Efrima, S. *J. Phys. Chem.* **1992**, *96*, 8469.
(37) Remacle, F.; Levine, R. D. *J. Phys. Chem. A* **2000**, *104*, 2341.
(38) Paldus, J.; Li, X. *Isr. J. Chem.* **1991**, *31*, 351.
(39) *The Unitary Group for the Evaluation of Electronic Energy Matrix Elements*; Lecture Notes in Chemistry; Hinze, J., Ed.; Springer: Berlin, 1981.
(40) Matsen, F. A. *Int. J. Quantum Chem.* **1974**, *S8*, 379.
(41) Coulson, C. A.; Fischer, I. *Philos. Mag.* **1949**, *40*, 386.
(42) Kim, S.-H.; Williams, S. R.; Heath, J. R. Private communication, 1999.
(43) Remacle, F.; Levine, R. D. Work in progress.